JOURNAL OF GEOPHYSICAL RESEARCH, VOL. 99, NO. A3, PAGES 3817-3826, MARCH 1, 1994

DMSP F8 observations of the mid-latitude and low-latitude topside ionosphere near solar minimum

M. E. Greenspan,[1,2] W. J. Burke,[3] F. J. Rich,[3] W. J. Hughes,[1] and R. A. Heelis[4]

The retarding potential analyzer on the DMSP F8 satellite measured ion density, composition, temperature, and ram flow velocity at 840-km altitude near the dawn and dusk meridians close to solar minimum. Nine days of data were selected for study to represent the summer and winter solstices and the autumnal equinox under quiet, moderately active, and disturbed geomagnetic conditions. The observations revealed extensive regions of light-ion dominance along both the dawn and dusk legs of the DMSP F8 orbit. These regions showed seasonal, longitudinal, and geomagnetic control, with light ions commonly predominating in places where the subsatellite ionosphere was relatively cold. Field-aligned plasma flows also were detected. In the morning, ions flowed toward the equator from both sides. In the evening, DMSP F8 detected flows that either diverged away from the equator or were directed toward the northern hemisphere. The effects of diurnal variations in plasma pressure gradients in the ionosphere and plasmasphere, momentum coupling between neutral winds and ions at the feet of field lines, and $\mathbf{E} \times \mathbf{B}$ drifts qualitatively explain most features of these composition and velocity measurements.

INTRODUCTION

In the topside ionosphere, both transport and chemical processes are important in determining the abundances and distributions of the ions O^+, H^+, and He^+. The most important chemical process is the resonant charge exchange reaction $H^+ + O \leftrightarrow O^+ + H$. Typically, O^+ is created by photoionization well below the 840-km altitude where measurements presented in this paper were made. H^+, then, is generated through charge exchange between neutral H and upgoing O^+. To a first approximation, the ratio $n[H^+]/n[O^+]$ is controlled by the height profiles of the neutral species. Transport, however, plays an important role. The direction and rate of transport of the two ion species depend strongly on the production rate of O^+ at low altitudes, the H^+ content on the flux tube in the protonosphere, the temperature profiles of the ion species, and the flux tube volume. Field-aligned components of the neutral wind at each foot of the flux tube, recombination of ions at low altitudes at night, and differences between production rates and scale heights in the conjugate ionospheres also play roles in driving transport [*Kutiev et al.*, 1980].

The results of these processes in the topside ionosphere have been investigated for many years, starting in the early days of the satellite era [*Brinton et al.*, 1969] and continuing to the present [*Heelis et al.*, 1990]. Direct measurements of ion density, composition, and motion are used both to test the outputs of thermospheric models and to provide realistic inputs to plasmaspheric models.

A much-studied feature of the topside ionosphere is the transition height, where $n[H^+] = n[O^+]$. The changes in the transition height with location, local time, season, activity, and phase of the solar cycle illustrate the dynamic nature of the ionosphere and the relative roles of chemistry and transport. Morphological studies of the transition level have been conducted at solar minimum by *Titheridge* [1976], using topside sounders, and by *Miyazaki* [1979], using satellite data. *Kutiev et al.* [1980] used satellite data to contrast the behavior of the transition height at solar maximum with that at solar minimum and to illustrate a strong longitudinal effect in the distribution of the topside ionospheric species at solar maximum. Further work on the ionosphere at solar maximum includes that of *Murphy et al.* [1984] and, more recently, *Heelis et al.* [1990]. Murphy et al. showed the strong influence that *F* region neutral winds have on the distribution of He^+ in the topside ionosphere. Heelis et al. further demonstrated that the combined effects of $\mathbf{E} \times \mathbf{B}$ drifts and neutral winds allow He^+ to become the dominant species at night in some regions of the topside, midlatitude ionosphere.

Extraordinarily detailed physical models of the interaction of the mid- to low-latitude ionosphere with the plasmasphere have been built up over the past two decades. Early models such as that of *Mayr et al.* [1967] solved the conservation of mass and energy equations for an ionosphere made up of O^+ and H^+ that was close to diffusive equilibrium. *Banks et al.* [1976] suggested that the topside ionosphere and the plasmasphere are strongly coupled through the interchange of H^+ ions which flow upward along magnetic field lines into the plasmasphere during the day and downward to the ionosphere at night. Recent models [*Richards and Torr*, 1985; *Bailey et al.*, 1987] include sources and sinks of the different species and the effects of Joule heating and of energetic photoelectrons that travel from the ionosphere to the plasmasphere or the conjugate ionosphere.

Direct observations of field-aligned flows of plasma into and out of the ionosphere have been reported from several spacecraft. Measurements from the ISIS 2 satellite at 1400 km showed that topside ions undergo outward, field-aligned

[1] Center for Space Physics, Boston University, Boston, Massachusetts.
[2] Now at Physics Department, University of Maryland, College Park.
[3] Phillips Laboratory, Hanscom Air Force Base, Massachusetts.
[4] Center for Space Sciences, University of Texas at Dallas, Richardson.

Paper number 93JA02287.
0148-0227/94/93JA-02287$05.00

streaming in response to magnetic activity [*Hoffman et al.*, 1974]. *Raitt and Dorling* [1976] discussed the global morphology of field-aligned ion flows, based on ESRO 4 observations near solar maximum. *Vickrey et al.* [1979] used incoherent scatter radar to measure the postsunset temporal variations in H^+ and O^+ fluxes.

This paper presents latitudinal distributions of the topside ionospheric species observed by the DMSP F8 satellite at solar minimum. DMSP F8 crosses the equatorial plane near dawn and dusk and therefore detects the transitional behavior characteristic of the topside ionosphere at these local times. The 98.7° inclination of the DMSP F8 orbit produces trajectories that cross some magnetic flux tubes that are sunlit and others that are in darkness. Despite the complications that result from this mixture of conditions, repeatable longitudinal variations appear in the observed latitudinal profiles. These highlight the influence of effects due to the dipole tilt in determining the distribution of the topside ionospheric species.

MEASUREMENT AND DATA REDUCTION TECHNIQUES

We present data acquired by the special sensor for ions, electrons, and scintillation (SSIES), a thermal plasma monitor on flight 8 of the Defense Meteorological Satellite Program series (DMSP F8). All DMSP spacecraft are three-axes-stabilized and have circular, sun-synchronous orbits at 840-km altitude and 98.7° inclination. DMSP F8 was launched on June 20, 1987. The ascending and descending nodes of its orbit are at 0600 and 1800 LT, respectively. With a period of 102 min, the ascending node moves westward 25.5° in geographic longitude per orbit, and the spacecraft makes 14.1 orbits per day. Figure 1 illustrates the relationship between the plane of DMSP F8's orbit, the various positions of the geomagnetic poles, and the ground terminator. Because of the inclination of the satellite's orbit, the spacecraft passes over a sunlit northern hemisphere and a dark southern hemisphere in June and a dark northern hemisphere and a sunlit southern hemisphere in both September and December.

The SSIES instrument on DMSP F8 comprises four sensors: an ion retarding potential analyzer (RPA), a total thermal ion density trap, an ion drift meter, and a spherical Langmuir probe for monitoring cold electrons [*Greenspan et al.*, 1986]. The three ion sensors have planar apertures that are mounted flush with a conducting plate. The sensor apertures and the plate are electrically coupled to form an equipotential plane, which is automatically biased away from the spacecraft frame potential to keep it close to the plasma potential [*Zuccaro and Holt*, 1982].

The geophysical parameters described in this study, that is, ion density, ion composition, and the downrange or ram component of the ion drift velocity, were obtained by analyzing RPA data. The RPA used a logarithmic electrometer to measure the current I of thermal ions that passed through its aperture as a function of retarding voltage V. The electrometer's range was 10^{-11} to 7×10^{-7} A. The retarding voltage swept between -3 V and $+12$ V with respect to the aperture potential every 4 s. Collected current was sampled 96 times during a sweep, with 24 samples per s. Each sampling period lasted 25 μs, during which V changed by $\sim 10^{-4}$ V. Uncertainty in the raw data due to instrument calibration and digitization is <2%. The spacecraft moved

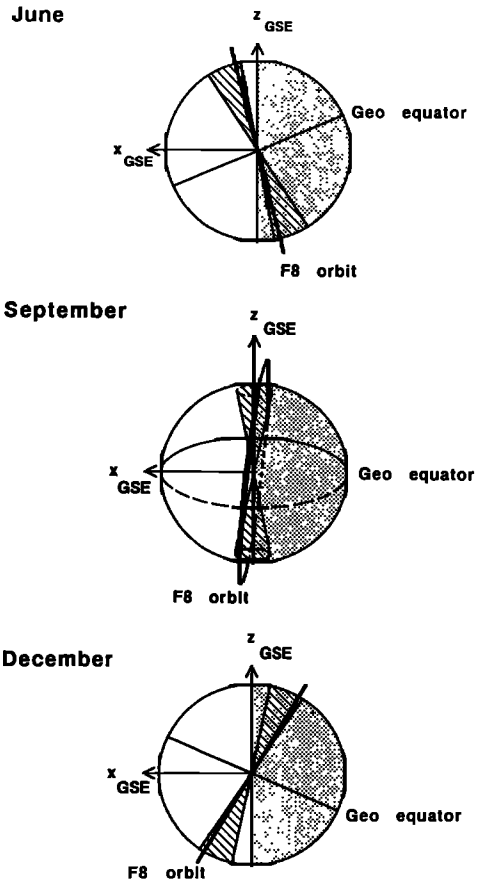

Fig. 1. Projection of DMSP F8's orbit (heavy line) on the GSE x-z plane at the June (top) and December (bottom) solstices and the September equinox (middle). The sunlit earth is white, and dark ground is grey. The striped cone indicates the range of angles that the projection of the magnetic pole on the GSE x-z plane sweeps through as the magnetic pole circles around the geographic pole each day. Dashed portions of the September dawn leg of the orbit, the geographic equator, and the locus of positions of the north magnetic pole are seen through the Earth.

30 km during each RPA sweep. Conditions in the equatorial and midlatitude regions usually vary little over this distance.

The geophysical parameters discussed in this paper are extracted from the $I(V)$ curves measured by the RPA. Under most conditions the light-ion concentration and the O^+ concentration can be obtained rather easily from the measured curve by examining the current near 0 V and the current near 3 V retarding potential, respectively. When two ion species are present, the ambient ion drift along the sensor look direction can be determined from the difference between the voltages where the light-ion current and the O^+ current to the RPA decrease most rapidly. This simple "pattern recognition" (PR) procedure uses very little computer time and generally provides measurements of the ion densities and the ratio of light ions to O^+, n[light]/n[O^+], with an accuracy better than 20% and of the ram drift with an estimated accuracy of 100 m/s. The PR code used in this work returned relative concentrations of O^+ and light ions and calculated the ion drift velocity only when n[light] $\geq$ 0.58 n[O^+], a conservative criterion. However, the code did not set an upper bound on the value of n[light]/n[O^+] for which the ion drift was calculated but instead tested for n[O^+] $\geq$ 80 cm^{-3}. Uncertainties in the reported drift velocity increase when O^+ is present but n[O^+] < 10^3 cm^{-3}.

It is also possible to utilize a nonlinear least squares fitting procedure to establish a best fit between measured and theoretical *I(V)* curves and thus to obtain the ambient ion drift velocity and the ion temperature. The least squares fitting procedure used in this work is the multidimensional downhill simplex method described by *Press et al.* [1986]. When using this procedure, we have assumed that the drift velocities and temperatures of all ion species are the same. The least squares fit, while utilizing more computer resources, provides ion drift and temperature data with errors of about 50 m/s and 5%, respectively. In addition, it provides a measure of the relative abundances of H^+ and He^+.

Regardless of the method of analysis, when the light-ion concentration drops to less than 1% of the O^+ concentration, it is no longer possible to determine the light-ion concentration accurately, and an estimate of the sensor plane potential with respect to the plasma is required to determine the ambient O^+ drift velocity. When the light-ion concentration is greater than 10% of the O^+ concentration, the least squares analysis indicates that the He^+ concentration is an order of magnitude or more less than the H^+ concentration. Thus under these conditions the topside composition and ram ion drift obtained by both methods are comparable.

Although we assume in both the PR and the least squares calculations that O^+ and light ions have the same ram drift velocity, the velocity calculated by our data reduction programs is essentially that of the O^+ ions. The calculated ion drift velocity depends on the difference between the voltages where the light-ion current and the O^+ current to the RPA decrease most rapidly. Because a shift in the O^+ velocity changes the O^+ energy in the spacecraft frame much more than a shift in the light-ion velocity changes the light-ion energy, this difference is far more sensitive to the O^+ velocity than to the light-ion velocity. For example, if the H^+ ion ram drift velocity $v_{H+} = -v_{O+}$, where v_{O+} is the O^+ ram drift velocity, the ion drift calculated assuming that both species have the same velocities is 1.13 v_{O+}. The observations of *Vickrey et al.* [1976] and the calculations of *Young et al.* [1979] suggest that in most cases the error in the O^+ velocity from assuming that O^+ and H^+ velocities are identical will be less than this.

Another source of error in the PR calculation of ion velocities is an ad hoc assumption that the light ions are 85% H^+ and 15% He^+. Results of the full least squares analysis and earlier measurements of ionospheric composition at solar minimum [e.g., *Taylor et al.*, 1968; *González et al.*, 1992] indicate that this is an upper bound on the fraction of He^+. If only H^+ is present, the assumption that 15% of the light ion population is He^+ means that the calculated velocities are too large by a factor of 1.03. The cumulative effects of the assumed H^+ to He^+ ratio and the assumption that $v_{H+} = v_{O+}$ will result in an error in the O^+ ram drift velocity of usually $\leq$16%.

OBSERVATIONS AND DISCUSSION

Data Selection

DMSP F8 RPA data are available from shortly after its launch in late June 1987 until the sensor failed on December 11, 1987. A 6-week hiatus occurred from mid July through August owing to difficulties with data acquisition software. To investigate the effects of magnetic activity and season, we examine 3 days with varied values of the daily sum of K_p ΣK_p as close as possible to each of the June and December solstices and to the September equinox. Table 1 lists the days along with ΣK_p and the flux of 10.7-m solar-radio emissions $F_{10\ 7}$ on each day. Because limited data were available in July and December and both months were unusually quiet, the "disturbed" solstice days are not very disturbed. Plots of the ion density, composition, and downrange drift were generated for the ascending and descending legs of every orbit on each of the days. To facilitate comparison of data acquired on different orbits and different days, we plotted geophysical parameters as functions of the subsatellite magnetic latitude. Then quantities such as the latitudes at which n[light] = n[O^+] were extracted from each plot and entered into a database.

Ion Density and Composition

Parameters in the database were taken from plots similar to those in Figures 2*a* and 2*b*. The figures show data taken during the three moderately active days listed in Table 1. Data displayed in Figure 2*a* were acquired in the morning, near 0600 LT, along ascending legs of DMSP F8 orbits, and those in Figure 2*b* were acquired in the evening, near 1800 LT, along descending legs of orbits. The H^+ and O^+ densities shown in Figure 2 were obtained by PR analysis. Dashed lines show the solar zenith angle at the spacecraft.

Measurements displayed in Figures 2*a* and 2*b* reveal characteristics of the data set as a whole. All orbits in the figures have regions where n[light] > n[O^+]. Regions of light-ion dominance along the DMSP F8 trajectories generally are not symmetric about the magnetic equator. They tend to appear in the dark, winter hemisphere near the solstices. Closer to equinox, light ions dominate near the equator but extend further into the dark northern hemisphere than into the sunlit southern hemisphere. Notice that variations in the ratio n[light]/n[O^+] primarily reflect variations in the latitudinal distribution of O^+. Near 840-km altitude, this species has much stronger latitudinal density gradients in the equatorial region than do light ions.

The complete set of total and light-ion density profiles used in this investigation is summarized in Figure 3*a* for the morning sector and Figure 3*b* for the evening sector. The nine daily summary plots are arranged as in Table 1, with each row representing a season and magnetic activity increasing from left to right within each row. This data set summary displays local time and seasonal and longitudinal dependencies. It suggests a magnetic activity dependence as well, particularly near the equinox.

In Figure 3 we see immediately that the hemispherical asymmetry in the location of regions of light-ion dominance

TABLE 1. K_p and $F_{10.7}$ on Study Days

	July	September	December
		Quiet Days	
Date	July 2, 1987	Sept. 19, 1987	Dec. 8, 1987
ΣK_p	6+	7−	2
$F_{10.7}$	72.0	82.0	91.4
		Average Days	
Date	July 8, 1987	Sept. 21, 1987	Dec. 3, 1987
ΣK_p	19−	18+	20+
$F_{10.7}$	73.6	82.4	88.3
		Disturbed Days	
Date	July 15, 1987	Sept. 25, 1987	Dec. 10, 1987
ΣK_p	28	38−	31−
$F_{10.7}$	76.3	77.5	92.9

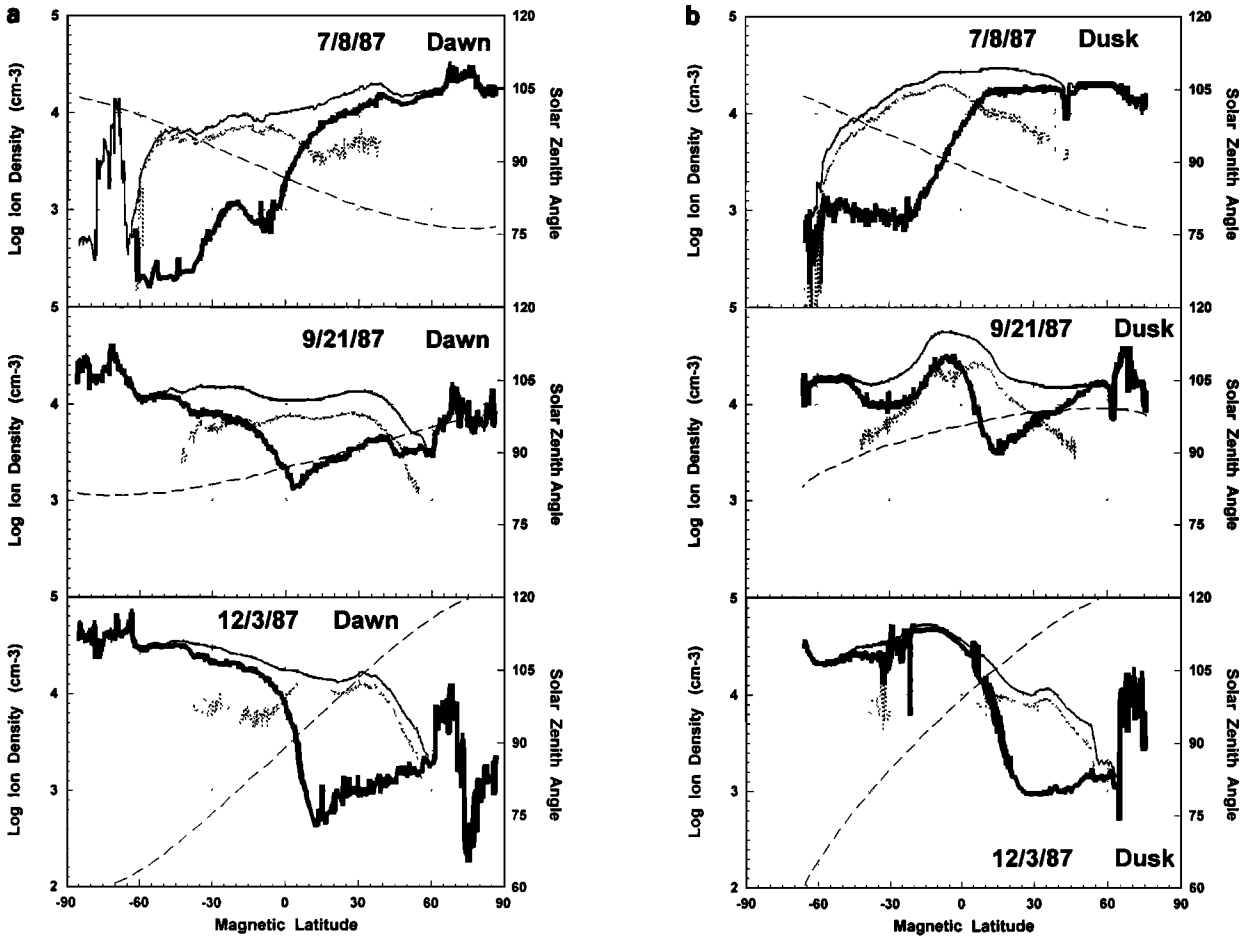

Fig. 2. Total ion (light solid curve), O^+ (heavy solid curve), and H^+ (dotted curve) densities as functions of magnetic latitude on moderately active days in July, September, and December 1987. The orbits cross the geographic equator at (a) ~65°E and 0130 UT near the dawn meridian and (b) ~60°E and 1400 UT near the dusk meridian. Dashed lines show the solar zenith angle at the satellite.

shown in Figure 2 is present in all the data. The asymmetry obviously shifts with season. The shift follows the seasonal shift in the region of the ionosphere beneath the spacecraft's orbit that is sunlit (see Figures 1 and 2). During the solstices, light ions tend to dominate in the entire dark, winter hemisphere in both morning and evening at all longitudes. At equinox the region of light ion dominance is more centrally located across the dip equator but usually extends farther into the dark northern hemisphere.

The regions of light-ion dominance are generally more extensive and more easily identified in the morning sector during all seasons. This is to be expected, as the transition height at a given local time depends not only on present circumstances but on previous conditions. Recombination of ions below the satellite during the night leads to downward diffusion and lower transition heights in the morning, while production of O^+ by photoionization at the ionospheric feet of the field lines and solar heating of the neutral atmosphere that raises the ratio of neutral O to H in the topside during the day both increase the transition altitude in the evening.

Note that the near-equinox days include the one truly disturbed day in our sample, September 25, 1987. The latitudinal extent of light-ion dominance on this day is smaller than on September 19 or 21, particularly in the morning sector. This increase in the transition altitude probably reflects the effects of Joule heating of the neutral atmosphere and enhanced upward transport due to emptying of plasmaspheric flux tubes. The larger effect of magnetic activity in the morning than the evening sector is to be expected, because increased energy deposition in the neutral atmosphere has a greater relative effect during the night than during the day, when sunlight is a major energy source.

It must be emphasized that the regions of light-ion dominance shown in Figure 3 reflect conditions near solar minimum at 840-km altitude. It should also be understood that the observed ion composition is strongly influenced by earlier plasma production, loss, and transport. Thus the morning side distributions largely result from processes taking place throughout the previous night, while the evening side distributions result from processes taking place throughout the previous day. These essential differences between the morning side and evening side data are most apparent near equinox, as Figure 4 illustrates.

Figure 4 shows the longitude-dependent variations in the O^+ and light-ion densities observed on the moderately active day September 21, near the dusk (Figure 4*a*) and dawn (Figure 4*b*) meridians. The equinoctial distributions of ion species are affected by prevailing $\mathbf{E} \times \mathbf{B}$ drifts and the displacement between the magnetic and geographic poles as well as by the different histories of the plasma at different

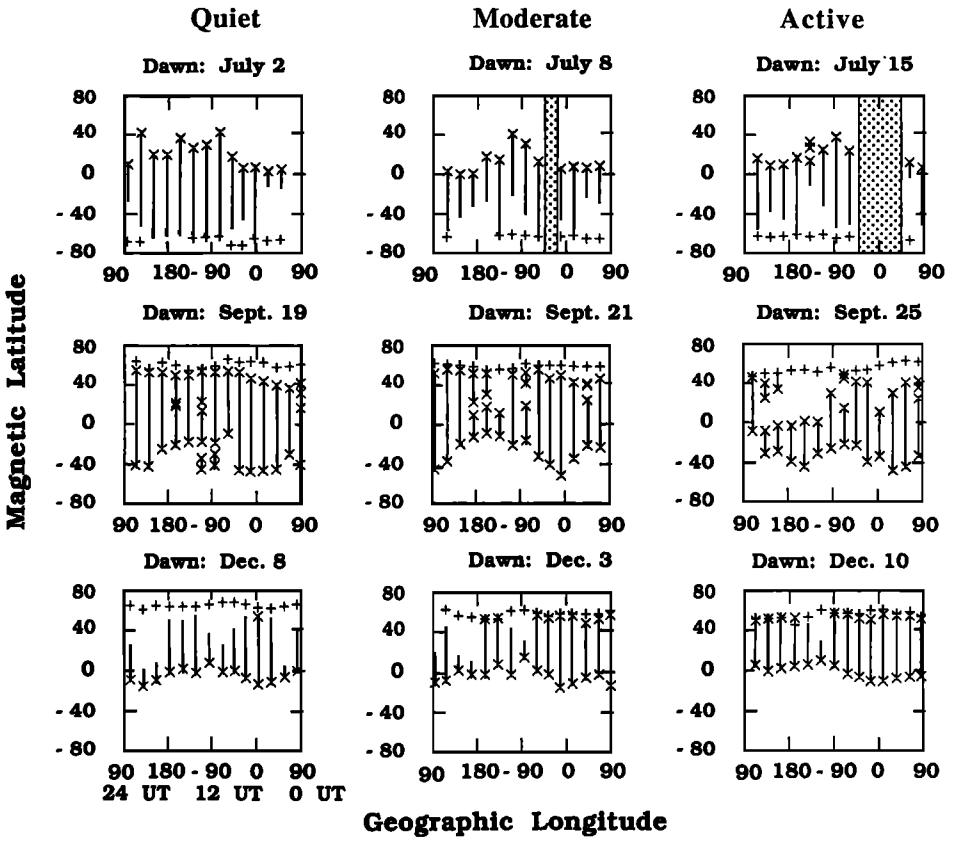

Fig. 3*a*. Summary of DMSP F8 measurements taken near the dawn meridian during the selected 9 days plotted on a geomagnetic latitude versus geographic longitude grid. Universal time increases from right to left within each plot, as indicated on the lower left hand plot. The location of the minimum total ion density on each orbit is marked with a plus sign, while crosses indicate transitions between regions of light-ion dominance and O^+ dominance. The vertical lines indicate regions of known light-ion dominance along each orbit. Missing crosses at one or both ends of a vertical line indicate that transitions from light-ion to O^+ dominance could not be located because of poor data quality or missing data. Shading indicates large data gaps.

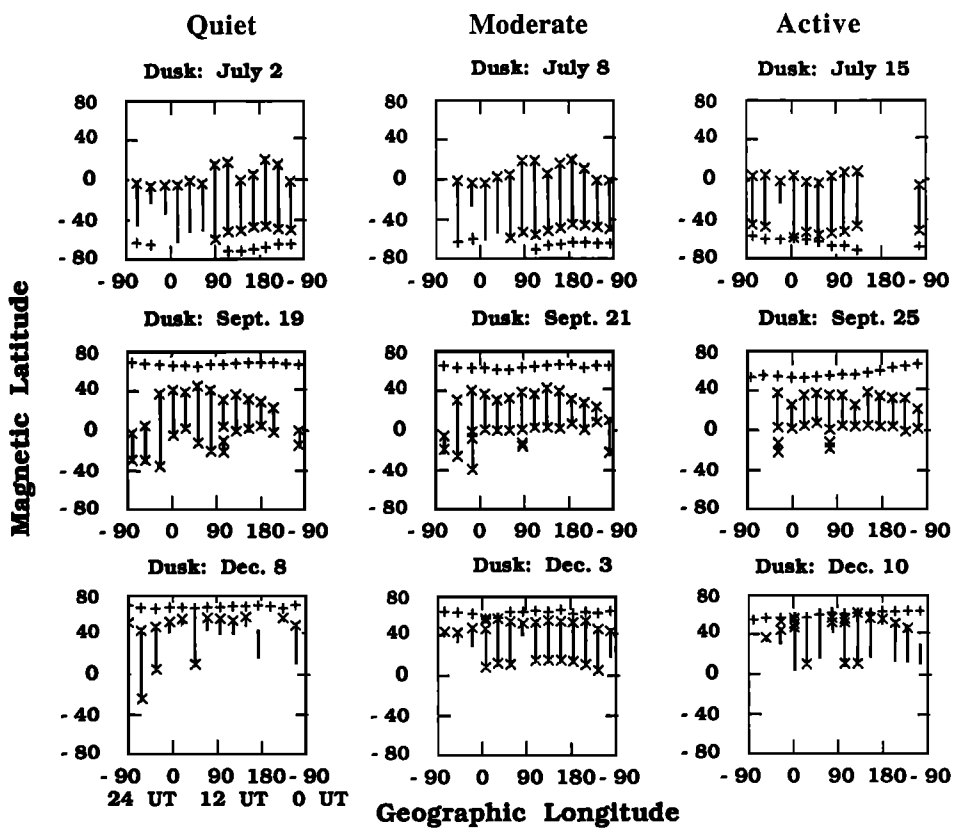

Fig. 3*b*. Summary of DMSP F8 measurements for the dusk meridian in the same format as that of Figure 3*a*.

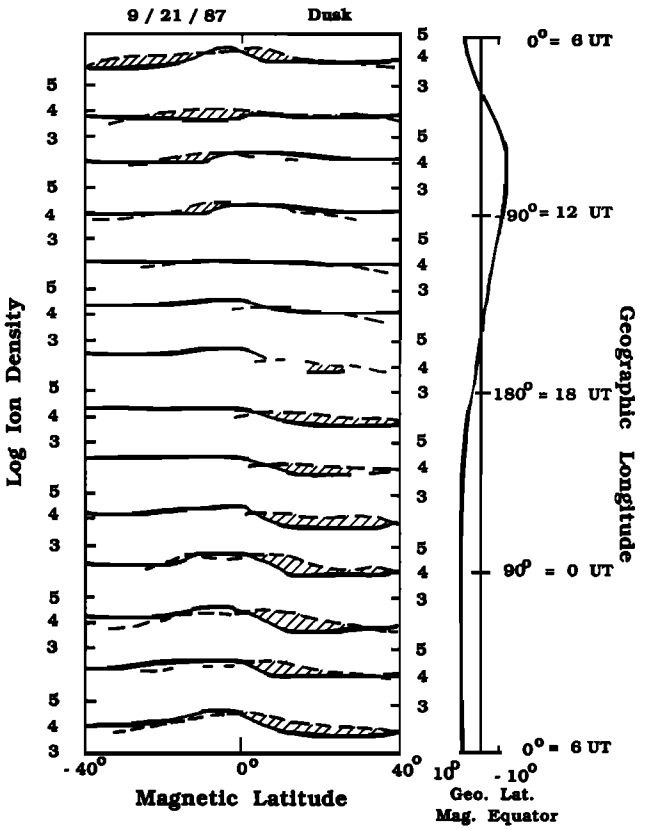

Fig. 4*a*. Logarithms of light-ion (dashed curves) and O^+ (solid curves) densities in cm^{-3} as functions of magnetic latitude taken near the dusk meridian on September 21, 1987. Shading indicates regions where n[light] > n[O^+]. Data were acquired during the 14 successive DMSP F8 orbits on the moderately active day September 21, 1987, within ±40° of the magnetic equator near the dusk meridian. The orbits are ordered by the geographic longitudes at which they crossed the magnetic equator, with increasing longitude running from bottom to top. The geographic latitude of the magnetic equator is shown as a function of geographic longitude at the right side of the figure.

local times. The displacement between the magnetic and geographic poles leads to different solar-zenith angles, neutral oxygen concentrations, and field-aligned neutral winds in the *F* region on flux tubes at different longitudes.

Near dusk (Figure 4*a*), the latitudinal profiles of O^+ reflect the processes that take place throughout the day, when the **E** × **B** drift is upward and the plasma transport processes along the magnetic field are dominated by the ion production rates in each hemisphere. Near the dip equator the vertical transport of 0^+ to high altitudes at dusk is controlled by upward **E** × **B** drifts and the 0^+-H^+ transition height remains near 800 km, while at higher latitudes, ion composition is modified drastically by field-aligned transport.

In the region between 0° and 160° longitude, the magnetic declination is small and the latitudinal distribution of composition is dominated by the displacement of the geomagnetic equator about 10° northward of the geographic equator. During the day, the integrated production rate in the north end of the flux tube is less than that in the south, and a south to north transport of plasma across the equator is produced. This asymmetry in the production rates and the subsequent interhemispheric transport is responsible for the latitudinal gradient in the O^+ concentration observed in this longitude region. The depressed O^+ concentration in the north leads to H^+ being the dominant ion at the spacecraft location in this region.

In the longitude region between −100° and −50°, the geomagnetic equator is south of the geographic equator and the flux-tube-integrated production rate in the south is less than that in the north, so a north to south transport of plasma occurs. In this region the O^+ concentration is depressed in the southern hemisphere and H^+ dominates at the spacecraft altitude. In the longitude regions near −160° and near −30°, the geomagnetic equator and the geographic equator are approximately collocated. In these regions the O^+ latitudinal distribution is quite symmetric and is more sensitive to the **E** × **B** drift history of the plasma.

The latitudinal concentration profiles observed near dusk decay after sunset, and processes acting throughout the night are responsible for the profiles seen near dawn. The variation in the relative abundances of O^+ and light ions near dawn is due largely to variability in the latitudinal distribution of O^+. In the morning, the profiles reflect the result of nighttime chemistry and transport processes. At the dip equator the O^+ concentration is reduced as the plasma **E** × **B** drifts downwards throughout the night. At latitudes farther from the equator, the decaying O^+ is replenished by downward diffusion of H^+ from high altitudes and subsequent charge exchange. Thus a local minimum in the O^+ at the dip equator is usually observed, but H^+ can become the dominant ion across the entire equatorial region.

Contrasting the density profiles shown in Figures 4*a* and

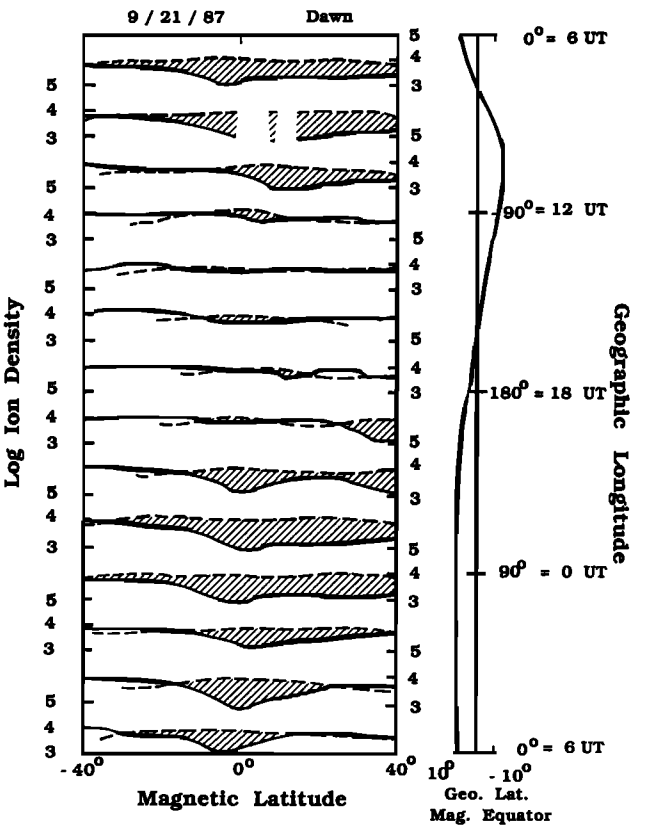

Fig. 4*b*. Profiles of light ion (dashed curves), and O^+ (solid curves) densities measured near the dawn meridian as functions of magnetic latitude and geographic longitude, presented in the same format as Figure 4*a*.

4*b*, we see that the changes in the light-ion profiles between evening and morning were not as dramatic as the changes in the O^+ profiles. This reflects both the large scale-height of ionospheric light ions and the fact that H^+ at 840 km has two possible sources. H^+ may move upward from lower altitudes after being created by charge exchange of neutral H with 0^+, or it may flow downward from the plasmasphere

While evening concentrations of light ions only slightly exceed morning concentrations at most longitudes, the difference is greatest between 0° and 90°E. There is a double-humped, equatorial-ionization-anomaly (EIA)-like signature in the light ion profiles in Figure 4*a* between 45° and 90°E, with the maximum O^+ density occurring between the two light-ion density peaks. It is possible that at these longitudes an evening upward $\mathbf{E} \times \mathbf{B}$ drift raises the equatorial transition altitude above DMSP F8's 840 km orbit and produces an equatorial peak in the O^+ concentration. H^+, starting at a higher altitude than O^+, would travel the same distance upward. Thus, it would be rise above DMSP F8 at the equator, and subsequently fall poleward along magnetic field lines, producing EIA-like peaks in the H^+ density profile where those field lines cross the spacecraft's orbit. The longitudes with the EIA-like signature at dusk are also those with deep, broad equatorial minima in the O^+ density at dawn. This hints that nighttime, downward equatorial $\mathbf{E} \times \mathbf{B}$ drifts that lead to loss of O^+ by recombination at low altitudes are strongest over the same longitude range. Similar effects were observed on the other two September days.

In the longitude region of small magnetic declination between 0° and 160°, the latitudinal asymmetry in the relative H^+ abundance is the same in the morning and evening. However, in the longitude region −60° to −10°, this asymmetry is reversed. This emphasizes the role of nighttime, zonal neutral winds that contribute only in regions where the magnetic declination is large. In this longitude region, where the field lines have a large westward declination, the day to night zonal wind has a strong component in the magnetic meridian from south to north at dawn. This tends to inhibit the decay of the O^+ in the south and produce a transport of H^+ from the south to the north. The observed latitudinal gradient in O^+ and the dominance of H^+ in the north at these longitudes are consistent with the presence of the neutral wind. At dusk at longitudes from −60° to −10°, the day to night zonal wind component along the magnetic meridian is directed north to south, congruent with the light-ion dominance in the south shown in Figure 4*a*.

DMSP F8 total density measurements taken near 0600 LT contrast with DMSP F2 observations taken 1 hour later in local time that show deep density minima near the equator. DMSP F8 measured total densities of the order of 10^4 cm^{-3} that remained nearly constant with latitude (see Figure 2). These values are roughly the same as those measured by DMSP F2 at the equator but a factor of 6 less than those DMSP F2 detected 10° to either side [*Burke et al.*, 1979]. We believe that the measurements presented here are consistent with the earlier observations and the interpretation of Burke et al.

Burke et al. suggest that the DMSP F2 profiles of total ion density versus latitude reveal the initiation of the daily cycle of flux tube refilling. Photoionization at sunrise generates overpressure in the *F* layer, causing both light ions and O^+ to flow upward along magnetic field lines. At relatively low altitudes the upward flow is limited to the O^+ ambipolar diffusion speed of ~1 km/s and creates an expanding front of denser plasma. The slant of magnetic field lines determines the altitude reached by the front at a given magnetic latitude at a given time after sunrise. Thus the DMSP F2 satellite, traveling at a constant altitude near the 0700 LT meridian, passed below the refilling front at midlatitudes and above it at equatorial latitudes. One hour earlier in local time, DMSP F8 detected plasma flowing toward the equator at <1 km/s (Figure 5*a*). The DMSP F8 measurements of mid- to low-latitude total ion densities were very close to the equatorial densities detected an hour later by DMSP F2, and the converging, field-aligned flows discussed in the next section have the values required by the expanding plasma front model.

Ram Velocity Measurements

The measurements of the downrange (ram) component of ion drift discussed below were made in regions where there were significant fractions of both light ions and O^+. It is in such regions that the ram drift can be most reliably determined from RPA current-voltage sweeps. As discussed above, although both H^+ and O^+ were present, the velocities determined from the RPA data reflect the O^+ velocity.

Figure 5 plots ram velocities measured within ±40° of the magnetic equator during three dawn passes near 65°E longitude and two dusk passes near 60°E longitude during the moderately active days listed in Table 1. Ion composition measurements for these passes are shown in Figure 2. We used the least squares analysis technique to determine the velocities plotted in Figure 5, where positive ram velocity indicates southward drift. The along-track component of corotation has not been subtracted from the data, nor has there been any attempt to "correct" measured velocities by assuming that they are projections of field- aligned flows onto the satellite track. The fluctuations in the velocities probably result from limitations of the analysis technique and from small changes in the ambient density or spacecraft potential during individual RPA sweeps.

In the morning, ram velocities were variable, with magnitudes up to ~700 m/s (Figure 5*a*). In all three cases the ram velocity changed sign at low latitudes: northward flows were observed in the southern hemisphere, and southward flows were observed in the northern hemisphere. In July, a strong, southward ion stream flowed away from the summer ionosphere across the magnetic equator. The direction reversed near the geographic equator (-8° magnetic latitude (MLAT)). At equinox, the largest northward flow occurred between the magnetic and geographic equators, with reversal of flow direction near the magnetic equator. In December, the largest northward flow was located 5° north of the magnetic equator. This may represent a transequatorial flow from the summer toward the winter hemisphere, with a weak southward flow poleward of 12° MLAT. In December, low densities of light ions in the sunlit summer hemisphere made it impossible to determine ram speeds poleward of -5° MLAT.

The behavior of the ram drift near dawn are summarized in Table 2, which gives the average latitudes Λ_{VMIN}, Λ_{V0}, and Λ_{VMAX} of minimum (northward), zero, and maximum (southward) ram velocities, respectively; the average minimum and maximum velocities V_{MIN} and V_{MAX}; and their standard deviations. In parentheses below each average is

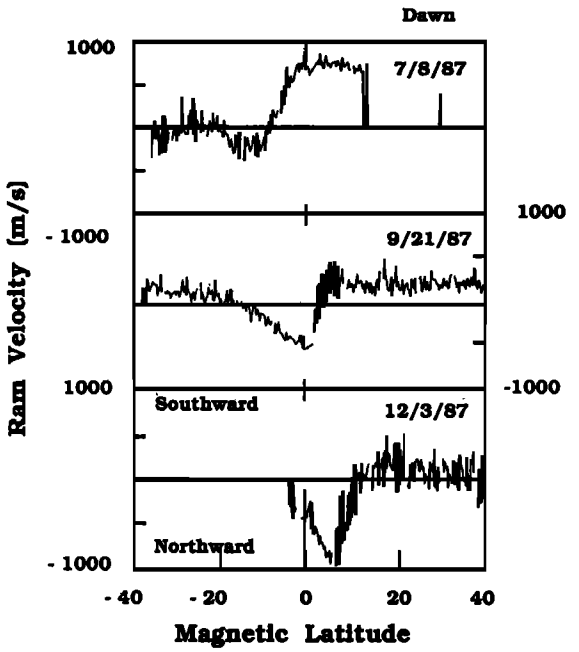

Fig. 5*a*. Ram component of the ion drift velocity measured on three dawn passes of DMSP F8 during the moderately active days in July, September, and December 1987 near 65°E.

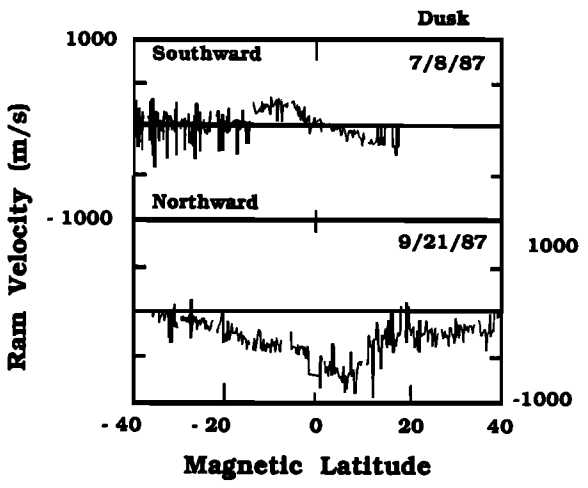

Fig. 5*b*. Ram component of the ion drift velocity measured on two dusk passes of DMSP F8 during the moderately active days in July and September 1987 near 60°E.

the number of passes used to determine it. Velocity statistics in Table 2 were determined from PR fits to RPA current-voltage curves. July values for Λ_{VMIN} and V_{MIN} could not be ascertained because only light ions were detected in the southern hemisphere.

Table 2 bears out the trends shown in the individual orbit plots of Figure 5*a*. Despite considerable scatter, it is clear that the average latitudes of the velocity minimum, null, and maximum shift toward the dark, winter hemisphere. Maximum southward velocities are largest in July and smallest in December, while maximum northward velocities are larger in December than in September. Ion temperatures determined by the PR technique have large scatter and uncertain reliability and are not shown here. However, in the morning the PR-determined ion temperature reaches a maximum near the equator at dawn, and, like the average latitudes of the velocity maximum, minimum, and null, the location of the temperature maximum shifts with season toward the winter hemisphere.

Examples of downrange velocities measured near the dusk meridian are shown in Figure 5*b*. In the July case, the ram drift reversed, indicating a divergence just north of the magnetic equator. The ram drift fell to near zero a few degrees south of the geographic equator. However, in the September example, the flow was always northward, away from the southern hemisphere across the magnetic and geographic equators. The patterns shown in Figure 5*b* are typical of July and September ram drift observations. In December the densities of light ions were too low near the magnetic equator to allow ram flow measurements.

In the evening we either observed plasma flowing northward in the northern hemisphere and southward in the southern hemisphere, with a ram velocity null near the equator, as shown in the top panel of Figure 5*b*, or plasma flowing northward across the equator, as in the bottom panel. In July, poleward flow from the equator was seen in 17 cases and northward transequatorial flow was seen in 14 of the 34 passes analyzed, while 3 cases could not be classified. In September there were 2 cases of poleward flow, 26 cases of northward flow across the equator, and 14 of 42 cases with velocity data quality too poor to classify. Because of the absence of appreciable light-ion concentrations near the equator at dusk in December, it was not possible to determine typical December ram flow patterns.

For two reasons, we believe that close to the equator, DMSP F8 ram velocity measurements primarily reflect field-aligned flows. First, at 840 km altitude, within ±15° of the magnetic equator, magnetic field lines are nearly parallel to the Earth's surface, with very small radial and azimuthal components. In this latitude range, the velocities of polar-orbiting satellites such as DMSP F8 have a large component parallel to the magnetic field lines. Second, measured ram speeds were typically in the 100 to 700 m/s range. At low latitudes, the plasma velocity transverse to the Earth's magnetic field, due to $\mathbf{E} \times \mathbf{B}$ drift, is typically a few tens of m/s or less [*Woodman*, 1970], and the ram component of the corotation velocity is about 80 km/s northward at the geographic equator, decreasing with latitude, while modeled field-aligned ion fluxes near dawn and dusk imply velocities in the hundreds of m/s range [*Bailey et al.*, 1987].

In this context, we interpret flows converging toward the equator from both sides in the morning as O^+ that has been created by photoionization near the feet of the field lines flowing upward to replenish the equatorial O^+ population that was depleted during the night by charge exchange and downward $\mathbf{E} \times \mathbf{B}$ drifts. Greater fluxes of O^+ are expected to come from the foot of the field line that receives more sunlight, thus producing the seasonal changes in Λ_{VMIN}, Λ_{V0}, Λ_{VMAX}, V_{MIN}, and V_{MAX} shown in Table 2.

Our RPA analysis codes assume that the plasma has a single, uniform flow velocity. It is possible that the large temperatures reported by the PR code near Λ_{V0} result when the code attempts to fit RPA *I(V)* curves due to counter-streaming O^+ from conjugate ionospheres to a curve that would be produced by a single ion distribution with a uniform, low ram flow speed. The off-equatorial flow energy of the O^+ is not sufficient to account for the apparent temperature increases.

TABLE 2. Seasonal Ram Velocity Characteristics

Month	Λ_{VMIN}	Λ_{V0}	Λ_{VMAX}	V_{MIN}	V_{MAX}
July		$-10.3° \pm 5.0°$	$-1.0° \pm 4.6°$		860 ± 230
	(0)	(4)	(14)	(0)	(14)
Sept.	$-7.1° \pm 5.7°$	$-5.1° \pm 7.4°$	$-4.6° \pm 6.4°$	-270 ± 210	580 ± 120
	(34)	(27)	(34)	(34)	(34)
Dec.	$4.0° \pm 4.5°$	$8.0° \pm 4.2°$	$15.3° \pm 4.7°$	-360 ± 260	390 ± 100
	(28)	(16)	(9)	(28)	(9)

Numbers in parentheses are numbers of passes used to determine values. Velocities in m/s.

The flow patterns observed in the evening are not easy to explain. Northward directed flows across the magnetic equator were dominant in September and occurred in a large minority of the July cases. These flows might be expected when the northern foot of a field line is in darkness and the southern foot is sunlit or at longitudes where the point on a field line with the smallest solar zenith angle at local noon is south of the magnetic equator and ion production is consequently larger on the southern half of the field line. Both of these conditions occur over most longitudes in September but not close to the June solstice. (See Figure 1 and the plot of geographic latitude of the magnetic equator in Figure 4). One would expect flows of O^+ directed away from the equator toward both poles, seen frequently in July, if ionization decayed at similar rates at both feet of the field lines. However, Figures 1 and 2 show that field lines crossed at northern latitudes in July are sunlit and those crossed at southern latitudes are dark. We cannot rule out the possibility that undetected systematic errors in the data reduction software or undetected spacecraft-plasma interactions play a role in creating the velocity patterns of Figures 5*a* and 5*b*.

SUMMARY AND CONCLUSIONS

In the previous section we presented measurements from the retarding potential analyzer on the DMSP F8 satellite taken near the dawn-dusk meridian under solar minimum conditions. To provide information about topside variations of ion composition and ram speed with magnetic latitude, longitude, season, and level of geomagnetic activity, 9 days of data were selected for study. Analysis of ion density observations focused on the ratio of light- to heavy-ion species at mid- to low latitudes as a function of longitude and activity as well as of latitude and season. Examination of ion drifts focused on their gross variation with latitude and season.

The most noticeable feature in our data set was the variation in ion composition near dawn and dusk at the altitude of DMSP F8's orbit. Ion data contained in Figures 2 through 4 demonstrate this variability. Light ions usually predominated at 840 km above the dark, winter ionosphere (Figures 2 and 3). During any given season we found remarkable day to day consistency in the DMSP F8 measurements. Clear variations with longitude and magnetic activity were evident. Quite frequently, the transition from heavy- to light-ion dominance occurred at or below 840 km. This contrasts with early observations reported by *Brinton et al.* [1969] and recent calculations by *Horwitz et al.* [1990] which, under solar maximum conditions, place the transition altitude above 1500 km. The DMSP observations, however, agree in general with *Titheridge*'s [1976] analysis of electron density profiles near solar minimum and with the solar minimum results of *Miyazaki* [1979]. Those studies showed that near the equator, transition heights may remain below 840 km at all local times. Both studies measured nightside transition heights as low as 660 km.

Field-aligned transport driven by a combination of pressure gradients and neutral winds combines with cross-field $\mathbf{E} \times \mathbf{B}$ drifts to qualitatively explain most longitudinal variations in the relative distribution of light and heavy ions at 840 km at dawn and dusk (Figure 4). The field-aligned plasma flows measured by DMSP F8 are signatures of this transport (Figure 5). During the day, downward pressure gradients and upward transport are generated by enhanced production of ions in regions that have larger neutral densities and receive more sunlight. At night, recombination at low altitudes creates upward pressure gradients and downward transport. Near the equator, minima in the O^+ concentrations at dawn and EIA-like signatures in the H^+ concentration at dusk probably are produced by $\mathbf{E} \times \mathbf{B}$ drifts. The longitudinal variation in these signatures suggests that the magnitude of the $\mathbf{E} \times \mathbf{B}$ drifts depends on longitude as well.

Acknowledgments. The authors wish to express their gratitude to Michael Mendillo for his many helpful comments on the significance and presentation of the DMSP F8 measurements presented here. One author (M.G.) wishes to thank S. Christon for helpful comments as well. The work was supported in part by Air Force contracts F19628–90–K–0002 with the University of Texas at Dallas and F19628–90–K–0003 with Boston University.

The Editor thanks P. G. Richards and another referee for their assistance in evaluating this paper.

REFERENCES

Bailey, G. J., P. A. Simmons, and R. J. Moffet, Topside and interhemispheric ion flows in the mid-latitude plasmasphere, *J. Atmos. Terr. Phys., 49*, 503–519, 1987.

Banks, P. M., R. W. Schunk, and W. J. Raitt, The topside ionosphere: A region of dynamic transition, *Annu. Rev. Earth Planet. Sci., 4*, 381, 1976.

Brinton, H. C., R. A. Pickett, and H. A. Taylor, Jr., Diurnal and seasonal variations of atmospheric ion composition: Correlation with solar zenith angle, *J. Geophys. Res., 74*, 4064–4073, 1969.

Burke, W. J., R. C. Sagalyn, R. G. Rastogi, M. Ahmed, F. J. Rich, D. E. Donatelli, and P. J. L. Wildman, Postsunrise refilling of the low- latitude topside ionosphere, *J. Geophys. Res., 84*, 4201–4206, 1979.

González, S. A., B. G. Fejer, R. A. Heelis, and W. B. Hanson, Ion composition of the topside equatorial ionosphere during solar minimum, *J. Geophys. Res., 97*, 4299–4304, 1992.

Greenspan, M. E., P. B. Anderson, and J. M. Pelagatti, Characteristics of the thermal plasma monitor (SSIES) for the Defense Meteorological Satellite Program (DMSP) spacecraft F8 through F10, *Rep.* AFGL–TR–86–0227, Hanscom Air Force Base, Mass., 1986.

Heelis, R. A., W. B. Hanson, and G. J. Bailey, Distributions of He^+ at middle and equatorial latitudes during solar maximum, *J. Geophys. Res., 95*, 10313–10,320, 1990.

Hoffman, JH., W. H. Dodson, C. R. Lippincott, and H. D. Hammack, Initial ion composition results from the Isis 2 satellite, *J. Geophys. Res., 79*, 4246–4251, 1974.

Horwitz, J. L., R. H. Comfort, P. G. Richards, M. O. Chandler, C. R. Chappell, P Anderson, W. B. Hanson, and L. H Brace, Plasmasphere-ionosphere coupling, 2, Ion composition measurements at plasmaspheric and ionospheric altitudes and comparison with modeling results, *J. Geophys. Res., 95*, 7949–7959, 1990.

Kutiev, I., R. A. Heelis, and S. Sanatani, The behavior of the O^+-H^+ transition level at solar maximum, *J. Geophys. Res., 85*, 2366–2372, 1980.

Mayr, H. G., L. H. Brace, and G. S. Dunham, Ion composition and temperature in the topside ionosphere, *J. Geophys. Res., 72*, 4391–4404, 1967.

Miyazaki, S., Ion transition height distribution obtained with the satellite Taiyo, *J. Geomagn. Geoelectr., 31*, 113, 1979.

Murphy, J. A., A. E. Sutton, and R. A. Heelis, The influence of neutral winds on He^+ distributions in the equatorial ionosphere, *Planet. Space Sci., 32*, 543, 1984.

Press, W. H., B. P. Flannery, S. A. Teukolsky, and W. T. Vetterling, *Numerical Recipes*, pp. 289-293, Cambridge University Press, New York, 1986.

Raitt, W. J., and E. B. Dorling, The global morphology of light ions measured by the ESRO-4 satellite, *J. Atmos. Terr Phys., 38*, 1077–1083, 1976.

Richards, P. G., and D. G. Torr, Seasonal, diurnal, and solar cycle variations of the limiting H^+ flux in the earth's topside ionosphere,*J. Geophys. Res., 90*, 5261–5268, 1985.

Taylor, H. A., Jr., H. C. Brinton, M. W. Pharo III, and N. K. Rahman, Thermal ions in the exosphere: Evidence of solar and geomagnetic control, *J. Geophys. Res., 73*, 5521–5533, 1968.

Titheridge, J. E., Ion transition heights from topside electron density profiles, *Planet. Space Sci., 24*, 229–245, 1976.

Vickrey, J. F., W. E. Schwartz, and D. T. Farley, Incoherent scatter measurements of ion counterstreaming, *Geophys. Res. Lett., 3*, 217–220, 1976.

Vickrey, J F., W. E. Schwartz, and D. T. Farley, Postsunset observations of ionospheric-protonospheric coupling at Arecibo, *J. Geophys. Res., 84*, 1310–1314, 1979.

Woodman, R. F., Vertical velocities and east-west electric fields at the magnetic equator, *J. Geophys. Res., 75*, 6249–6259, 1970.

Young, E. R., D. G. Torr, and P. G. Richards, Counterstreaming of O^+ and H^+ ions in the plasmasphere, *Geophys. Res. Lett., 6*, 925–928, 1979.

Zuccaro, D., and B. J. Holt, A technique for establishing a reference potential on satellites in planetary ionospheres, *J. Geophys. Res., 87*, 8327–8329, 1982.

W. J. Burke and F. J. Rich, Phillips Laboratory, Hanscom AFB, MA, 01731. (e-mail: Internet.burke@plh.af.mil and Internet.rich@plh.af.mil).

M. E. Greenspan, Physics Department, University of Maryland, College Park, MD 20742. (e-mail: Internet.greenspan@umdspa.umd.edu).

R. A. Heelis, Center for Space Sciences, University of Texas at Dallas, Box 830688, M/S F022, Richardson, TX 75083. (e-mail: Internet.heelis.utdallas.edu).

W. J. Hughes, Center for Space Physics, Boston University, Boston, MA 02215. (e-mail: Internet.hughes@buasta.bu.edu).

(Received October 19, 1992;
revised July 8, 1993;
accepted August 6, 1993.)